

B-9-5

Highly Reliable DRAM Technology for ASM with Dual Nitrogen Concentration Gate Oxynitrides using Selective Nitrogen Implantation

Taro Sugizaki, Atsushi Murakoshi*, Tetsu Tanaka, Ryota Katsumata*, Toshiro Nakanishi, and Yasuo Nara

Fujitsu Laboratories Ltd., 10-1 Morinosato-Wakamiya, Atsugi-shi, Kanagawa 243-0197, Japan

Phone: +81-46-250-8215 Fax: +81-46-250-8804 E-mail: sugizaki@jp.fujitsu.com

*Toshiba Corporation, 8 Shinsugita-cho, Isogo-ku, Yokohama 235-8522, Japan

Abstracts

A poly-metal dual gate DRAM for ASM (Application Specific Memory) with dual nitrogen concentrated oxynitrides was developed for the first time. This technology uses selective nitrogen implantation just after gate oxidation. The nitrogen concentration of PMOS in gate dielectric combined with nitrogen implantation and NO annealing is high enough to suppress boron penetration. The nitrogen concentration of Cell-Tr and NMOS is low enough to keep V_{th} without increasing channel dose by using only NO annealing. This method improves oxynitride reliability due to $Si_3 \equiv N$ formation instead of SiO_xN_y bonds.

Introduction

Recently, DRAM market needs ASM such as mobile FCRAM instead of conventional DRAM. Poly-metal dual gate is expected to be applied in next-generation ASM to achieve high-speed, low voltage and low power operation, but poly-metal dual-gate FCRAM suffer from a severe thermal budget. Therefore, PMOS gate oxides require a high nitrogen concentration to suppress boron penetration. A high nitrogen concentration, however, shifts V_{fb} , and decreases V_{th} of both NMOS and Cell-Tr, leading to an off current increase and a resultant retention time failure. Thence it is impossible to optimize nitrogen concentration of Cell-Tr and PMOS at the same nitrogen concentration (Fig. 1).

There are reports about nitrogen implantation for suppressing boron penetration [1,2]. However, nitrogen implantation into gate electrodes causes gate poly-Si depletion because B-N bonds are generated and, nitrogen implantation into the silicon substrate before gate oxidation causes a degradation of gate oxide reliability. In addition, these papers do not mention the issue of V_{th} -decrease in NMOS and Cell-Tr.

We developed a method of selective nitrogen implantation that is performed just after gate oxidation. In our method, nitrogen is implanted into only the PMOS region, and nitrogen concentration of PMOS and Cell-Tr can be controlled independently.

Fabrication process

Figure 2 shows process flow for dual nitrogen-concentrated gate oxynitrides. After STI formation, gate oxides were grown in a furnace, and this was followed by resist patterning at only the NMOS region. Then nitrogen was implanted into only PMOS region through gate oxides at a dose ranging from $5E14$ to $1E15$ cm^{-2} . NO annealing was then carried out in a temperature range of $800^{\circ}C$ to $900^{\circ}C$. Table 1 shows split conditions. Next, poly-metal gate, consisting of poly-Si, WN_x and W, was deposited. A sidewall and source-drain were then formed after the LDD. After that, activation annealing was performed at $1000^{\circ}C$ for 5s. Finally, sintering was carried out at N_2/H_2 ambient.

Results and Discussion

1. Gate dielectric properties

First, we investigate the gate dielectric characteristics. Figure 3 shows nitrogen depth profiles measured with SIMS. The nitrogen-implanted samples have the same peak position as the control sample. The nitrogen atoms of all samples pile up at

the Si/SiO_2 interface. Figure 4 shows N1s core level spectra obtained by XPS. All samples have peaks at about 398 eV. These peaks correspond at the $Si_3 \equiv N$ bond. A SiO_xN_y bond at about 399 eV was not observed. These results show that the nitrogen-implanted samples have the same properties as control sample.

In order to evaluate boron penetration, boron depth profiles were measured with backside SIMS, as shown in Fig. 5. These results show that boron penetration is suppressed in nitrogen-implanted samples, comparing with the control sample. Nitrogen implantation of $1E15$ cm^{-2} suppresses boron penetration completely.

2. Electrical characteristics

Figure 6 shows the V_{th} - I_{on} characteristics for Cell-Tr. V_{th} of $850^{\circ}C$ -NO sample is 140mV higher than that of $900^{\circ}C$ -NO sample. This result leads to improved off-current.

To evaluate boron penetration, PMOS V_{th} variations were measured under different oxynitridation conditions. V_{th} variations of nitrogen-implanted samples are smaller than that of control sample. Nitrogen implantations of $1E15$ cm^{-2} have minimal V_{th} variation (Fig. 7). This result suggests that nitrogen implanted samples suppress boron penetration. Nitrogen implantations of $1E15$ cm^{-2} suppress boron penetration completely.

Figure 8 shows V_{th} dependence on nitrogen concentration. Hatched areas indicate appropriate nitrogen concentration for Cell-Tr and PMOS, respectively. The Cell-Tr needs NO annealing below $850^{\circ}C$ for reducing off-current. The PMOS needs NO annealing above $800^{\circ}C$ with nitrogen dose larger than $5E14$ cm^{-2} for suppressing boron penetration. The conditions with a nitrogen dose of $1E15$ cm^{-2} and NO annealing of $800^{\circ}C$ satisfied both off-current and boron penetration requirements, simultaneously.

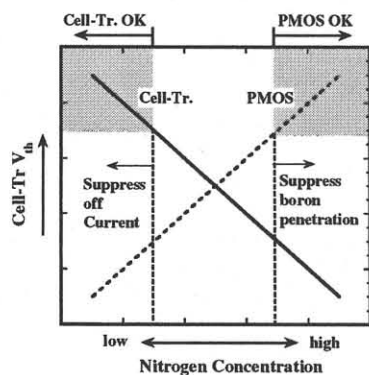
Figure 9 shows TDDDB characteristics under different oxynitridation conditions. In the p^+ gate, nitrogen-implanted samples improved the TDDDB lifetime. In the previous study [2], nitrogen implantations were performed before gate oxidation. This method degrades oxide reliability. We speculate that this degradation was caused by formed SiO_xN_y bonds. In this work, nitrogen implantations were performed after gate oxidation. This method improves oxide reliability due to $Si_3 \equiv N$ bonds and no SiO_xN_y bonds (Fig. 4).

Conclusions

We have newly developed DRAM technology for ASM with gate oxides having different nitrogen concentrations between Cell-Tr and PMOS in a poly-metal dual-gate FCRAM. We found the optimum conditions to be $N^+ 1E15$ $cm^{-2} + 800^{\circ}C$ -NO. Under this condition, PMOS V_{th} variations were successfully decreased to suppress boron penetration and the large increases of V_{th} in NMOS and Cell-Tr resulting from low nitrogen concentrations. We have realized a poly-metal dual-gate FCRAM that has high-performance PMOS, NMOS, and Cell-Tr without degrading oxide reliability.

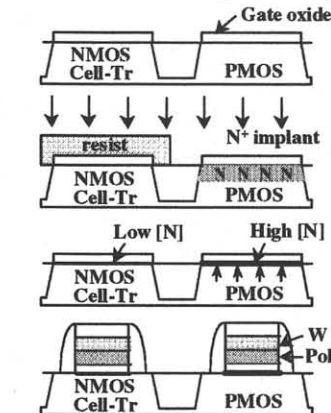
References

- [1] T.Kuroi et.al., VLSI symp. Tech. Dig., p.107, 1994
- [2] Y.Y.Chen et.al., IEDM Tech. Dig., p.639, 1997



It is impossible to optimize [N] of PMOS and Cell-Tr at the same concentration. Hatched areas indicate appropriate region.

Fig. 1 Concept for dual nitrogen concentration gate oxynitrides



- Gate oxidation
wet-ox 3.5 nm
- Resist patterning
- Nitrogen implantation
3keV, 0 to 1E15 cm⁻²
- Resist strip
- NO annealing
800, 850, 900 °C
- Gate electrode deposition
- Activation anneal
1000 °C 5s

Fig. 2 Process flow for dual concentration oxynitrides. Nitrogen was implanted just after gate oxidation. The N concentration of PMOS is higher than that of NMOS and Cell-Tr.

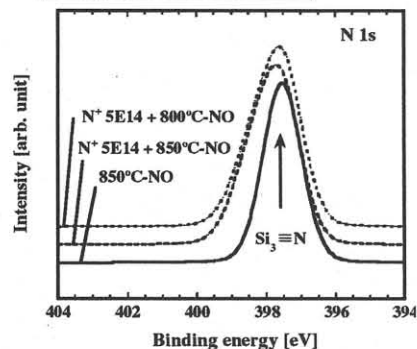


Fig. 4 N1s core level spectra in gate oxynitrides obtained by XPS. Si₃≡N bonds are only observed.

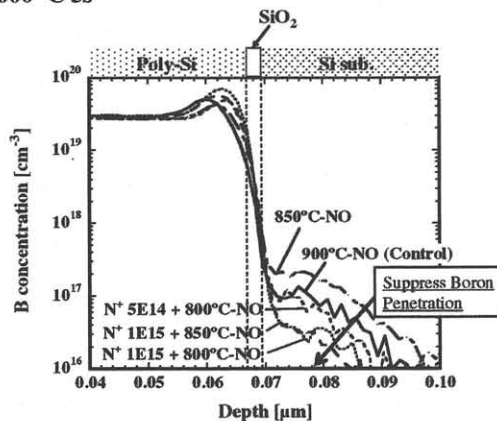


Fig. 5 Boron depth profiles with p⁺ polymetal gate samples obtained by SIMS. Boron atoms penetrate gate oxides into the Si substrate.

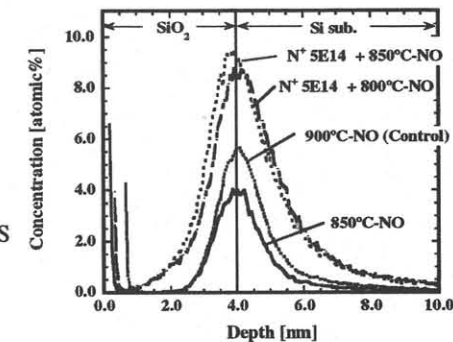


Fig. 3 Nitrogen depth profiles in gate oxynitrides obtained by SIMS. Nitrogen atoms pile up at Si/SiO₂ interface.

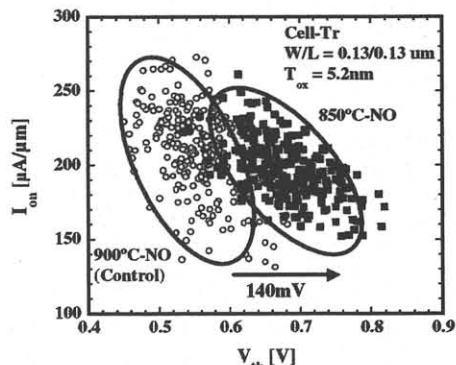


Fig. 6 V_{th}-I_{on} characteristics of Cell-Tr. Lower temperature oxynitride increases V_{th} of cell-Tr.

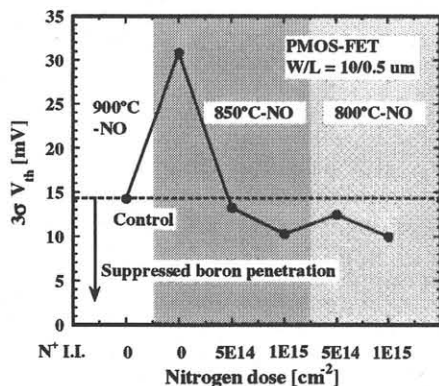


Fig. 7 PMOS V_{th} variation under different oxynitridation conditions.

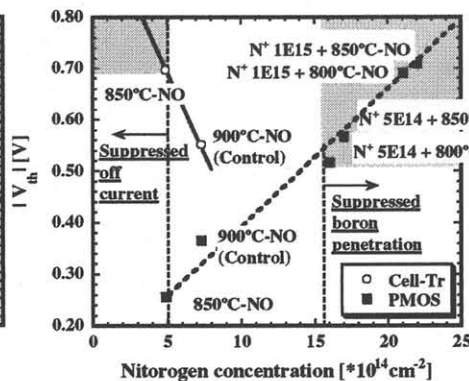


Fig. 8 PMOS and Cell-Tr V_{th} dependence on nitrogen concentration. Hatched areas indicate appropriate region.

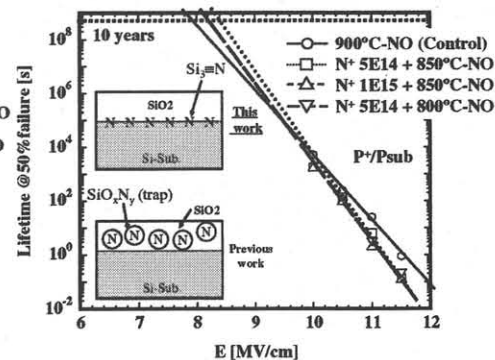


Fig. 9 TDDDB lifetime under different oxynitridation conditions with poly-metal p⁺ gate.

Table. 1 Split conditions

	Gate oxide	N ⁺ I.L. (only PMOS region)	NO anneal
1 (Control)	3.5 nm	----	900 °C
2	3.5 nm	----	850 °C
3	3.5 nm	5E14 cm ⁻²	850 °C
4	3.5 nm	1E15 cm ⁻²	850 °C
5	3.5 nm	5E14 cm ⁻²	800 °C
6	3.5 nm	1E15 cm ⁻²	800 °C